6-12-2019

Quantifying Methane Emissions in the Uintah Basin During Wintertime Stagnation Episodes

C. S. Foster
The University of Utah

Erik T. Crosman
The University of Utah, Erik.Crosman@utah.edu

J. D. Horel
The University of Utah

Seth Lyman
Utah State University, seth.lyman@usu.edu

B. Fasoli
The University of Utah

R. Bares
The University of Utah

Recommended Citation

Foster, C.S., Crosman, E.T., Horel, J.D., Lyman, S., Fasoli, B., Bares, R. and Lin, J.C., 2019. Quantifying methane emissions in the Uintah Basin during wintertime stagnation episodes. Elem Sci Anth, 7(1), p.24. http://doi.org/10.1525/elementa.362

ELEMENTA
Science of the Anthropocene

Foster, CS, et al. 2019. Quantifying methane emissions in the Uintah Basin during wintertime stagnation episodes. *Elem Sci Anth,* 7: 24. DOI: https://doi.org/10.1525/elementa.362

RESEARCH ARTICLE

Quantifying methane emissions in the Uintah Basin during wintertime stagnation episodes

C. S. Foster*, E. T. Crosman*, J. D. Horel*, S. Lyman†, B. Fasoli*, R. Bares* and J. C. Lin*

This study presents a meteorologically-based methodology for quantifying basin-scale methane (CH_4) emissions in Utah's Uintah Basin, which is home to over 9,000 active and producing oil and natural gas wells. Previous studies in oil and gas producing regions have often relied on intensive aircraft campaigns to estimate methane emissions. However, the high cost of airborne campaigns prevents their frequent undertaking, thus providing only daytime snapshots of emissions rather than more temporally-representative estimates over multiple days. Providing estimates of CH_4 emissions from oil and natural gas production regions across the United States is important to inform leakage rates and emission mitigation efforts in order to curb the potential impacts of these emissions on global climate change and local air quality assessments. Here we introduce the Basin-constrained Emissions Estimate (BEE) method, which utilizes the confining topography of a basin and known depth of a pollution layer during multi-day wintertime cold-air pool episodes to relate point observations of CH_4 to basin-scale CH_4 emission rates. This study utilizes ground-based CH_4 observations from three fixed sites to calculate daily increases in CH_4, a laser ceilometer to estimate pollution layer depth, and a Lagrangian transport model to assess the spatial representativity of surface observations. BEE was applied to two cold-air pool episodes during the winter of 2015–2016 and yielded CH_4 emission estimates between $44.60 +/- 9.66 \times 10^3$ and $61.82 +/- 19.76 \times 10^3$ kg CH_4 hr^{-1}, which are similar to the estimates proposed by previous studies performed in the Uintah Basin. The techniques used in this study could potentially be utilized in other deep basins worldwide.

Keywords: Methane; Emissions; Oil; Natural gas

1 Introduction

Global methane (CH_4) levels have increased over the past several decades, with numerous studies attributing the rise at least partially to increased anthropogenic emissions (Bruhwiler et al. 2017; Miller et al. 2013; Nisbet et al. 2016; Saunois et al. 2016, 2017; Sheng et al. 2018; Thompson et al. 2018; Turner et al. 2016, 2017, 2019). One key anthropogenic CH_4 source is leakage of gases during oil and natural gas (ONG) extraction and processing activities. As a greenhouse gas, CH_4 is much more potent than carbon dioxide (CO_2), which means as more CH_4 is emitted through the processes associated with ONG production, processing, transmission, and storage, as well as from abandoned wells, its positive benefits can quickly be outweighed by its climate forcing (Kang et al. 2014; Howarth 2014).

The rapidly growing natural gas and petroleum industry is a large source of anthropogenic CH_4 in the US (Maasakers et al. 2016). The CH_4 leakage rates noted by mobile surface and aircraft studies across ONG production regions in the US have shown significant spatial variability (Karion et al. 2013, 2015, Peischl et al. 2015, 2016; Petron et al. 2012; Goetz et al. 2017; Connell et al. 2019), and emission inventories of CH_4 from ONG producing regions remain uncertain, with a recent survey study estimating current inventories underestimate CH_4 leak rates by 60% (Alvarez et al. 2018). It is well-known that CH_4 emissions from the ONG industry vary as a function of region, supply chain processes, and operational practices, but limited data exist to quantify these variations over time scales ranging from diurnal to decadal (Balcombe et al. 2018; Orellana et al. 2018). Improved understanding of the effect of ONG emissions on air pollution-related health impacts across the United States is also needed (Fann et al. 2018; Vaughn et al. 2018), as CH_4 is co-emitted with nitrogen oxide (NO_x) and volatile organic compounds (VOCs), key precursor pollutants for ozone and particulate pollution.

The many uncertainties in emissions estimates and observations highlight the work still needed to fully comprehend the role the ONG industry plays both locally (air quality) and globally (climate impacts). Numerous aircraft observational field campaigns (e.g., Caulton et al. 2014; Karion et al. 2013, 2015; Peischl et al. 2015, 2016; Barkley et al. 2017; Lavoie et al. 2017) have provided observations

* The University of Utah, Department of Atmospheric Science, Salt Lake City, Utah, US

† Utah State University, Bingham Research Center, Vernal, Utah, US

Corresponding author: E. T. Crosman (Erik.Crosman@utah.edu)

of CH_4 leak rates across large ONG production regions in the US. Airborne measurements are generally conducted during the daytime, during short (few day) field campaigns, and frequent sampling with aircraft is generally cost-prohibitive. While some studies have suggested that temporal variations in CH_4 emissions as small as on diurnal scales may be significant (Vaughn et al. 2018), measurements over the same regions over different time periods, with different methods, are generally lacking. Measurements over the same area over multiple years using all available methods would yield greater confidence in the estimated CH_4 emission rate from a given region, the representativeness of any one method, and trends in emissions.

The Uintah Basin of eastern Utah (hereafter and frequently referred to as the "Basin") is home to over 9,000 active and producing ONG wells alongside extensive production and transport infrastructure. Here, the large topographic relief, periodic surface snow cover, and strong capping static stability above the surface (a 'lid' that inhibits vertical atmospheric mixing) combine with ONG-related emissions to produce prolonged wintertime pollution episodes. These pollution episodes occur during a meteorological phenomenon known as "cold-air pools" (Lyman and Tran 2015), defined as cold air filling a topographic depression and occur when either surface cooling or warming aloft result in stable vertical stratification of the boundary-layer air that remains trapped laterally within the basin topography (Lareau et al. 2013). Cold-air pool conditions are favored under high atmospheric pressure, light winds, and low insolation. During cold-air pools, the Uintah Basin becomes a quasi-closed system in which pollutants accumulate within a shallow volume of air less than 500 m deep for periods ranging from several days to several weeks.

The Uintah Basin has been the topic of extensive research over the last decade regarding wintertime pollution episodes driven by emissions from ONG production building up within cold-air pools (Schnell et al. 2009; Edwards et al. 2014; Helmig et al. 2014; Yuan et al. 2016; Subramanian et al. 2015; Lyman and Tran 2015; Neemann et al. 2015; Matichuk et al. 2017; Tran et al. 2018). These cold-air pools and the associated build-up of boundary-layer pollution, along with the increased actinic flux and photochemical processes associated with the high reflectivity of snow cover during late winter, have also resulted in numerous documented exceedances of the National Ambient Air Quality Standard (NAAQS) for ozone within the Uintah Basin (Edwards et al. 2014; Koss et al. 2015; Mansfield and Hall 2018).

The Uintah Basin has been shown to be unique in terms of its large leakage rate of CH_4 from the ONG industry (Karion et al. 2013; Ahmadov et al. 2015). The Basin is also geographically situated in a favorable location to observe ONG-derived CH_4 emissions without significant contamination from urban, agricultural, or biogenic sources. For reasons that are currently unknown, the fugitive emission (leakage) of CH_4 through the processes of its extraction, storage, transportation, and distribution within the Uintah Basin has been found to be among the highest observed in the United States. Karion et al. (2013) found the leakage rate of CH_4 from ONG activity within the Basin to be roughly 8.9 +/− 2.7% (emissions as a percentage of natural gas production), which is generally several percentage points higher than most other ONG regions across the United States. Foster et al. (2017) confirmed the emission rate of Karion et al. (2013) using *in situ* CH_4 observations combined with a Lagrangian transport model and further showed that the US Environmental Protection Agency (EPA) CH_4 emission inventory (Maasakers et al. 2016) significantly underestimates emissions in the Uintah Basin. Analysis of CH_4 emissions from well pads by Robertson et al. (2017) also confirmed that leakage rates in the Basin (2.8%, or 1.0–8.6% at 95% confidence) were higher than other basins/plays, such as those observed in Fayetteville, Arkansas (0.09%), the Upper Green River, Wyoming (0.18%), and Denver-Julesburg, Colorado (2.1%). More recently, Omara et al. (2018) confirmed the Basin falls within the range of basins with high site-level emissions (2.2 kg/h/site), although it was not found to be the highest among the basins investigated. While continuous CH_4 measurements for two winters in the Uintah Basin were discussed by Helmig et al. (2014), to our knowledge Foster et al. (2017) was the first study to leverage CH_4 measurements at fixed ground-based sites to improve the understanding of Basin-scale emissions. The unique ongoing observations of CH_4 being collected as mole fractions (nanomoles of CH_4 per mole of dry air, in parts per billion ppb)) as part of a study funded by the National Oceanic and Atmospheric Administration that were utilized to validate model simulations in Foster et al. (2017) are utilized directly in this paper to estimate basin-scale emissions of CH_4.

While satellite data have been widely used to provide estimates over time of air quality across air sheds and basins (Duncan et al. 2014), this is the first study to our knowledge to utilize topography and meteorology to estimate basin-scale emissions from spatially distributed surface observations. In this study we present a simple methodology – the Basin-constrained Emissions Estimate (BEE) – to quantify basin-scale CH_4 emissions in Utah's Uintah Basin. BEE uses basin topography and meteorology in concert with spatially distributed *in situ* observations to estimate Uintah Basin CH_4 emissions. The multi-day build-up of CH_4 is investigated during two wintertime cold-air pools in the winter of 2015–2016. In Section 2, the data utilized and the BEE methodology are discussed. In Section 3, the results from applying the BEE methodology to two case studies in the winter of 2015–2016 are discussed. A summary and recommended future work are given in Section 4.

2 Data and Methods

2.1 Overview

The Basin-constrained Emissions Estimate (BEE) method utilizes the confining topography and shallow depth of wintertime pollution layers to relate spatially distributed point-source observations of CH_4 to basin-scale CH_4 emission rates. The Basin's topography confines its volume laterally, while strong boundary-layer static stability confines the basin volume vertically, resulting in a rela-

tively well-constrained volume in which emissions accumulate over multi-day pollution episodes. In Section 2.2, the BEE calculation is presented, followed by a description of the components that are needed to calculate BEE in Sections 2.3–2.7. In Section 2.3, the CH_4 observations from three locations in the Basin used to calculate daily rates of change are discussed. In Section 2.4, the ceilometer data and methodology for determining the vertical mixing depth and top of the polluted volume are presented. Section 2.5 elaborates on the uncertainty analysis for the BEE approach. Section 2.6 explains the setup of the Lagrangian transport model. Section 2.7 gives an overview of the two case studies highlighted in this paper. CH_4 atmospheric mole fractions are measured in ppb, while emission rate is generally expressed in kg CH_4 hr^{-1} on a Basin-wide scale.

2.2 Basin-constrained emissions estimate (BEE) approach

The BEE approach calculates the basin-scale emissions rate (E) using the following formula:

$$E = (\Delta\rho/\Delta t) * V = (\Delta\rho/\Delta t) * \sum_{i=1}^{n} (A_i * \Delta z_i) \quad \text{(Eq. 1)}$$

where $\Delta\rho/\Delta t$ is the density tendency of CH_4 calculated using observed CH_4 at each site over the time step Δt of interest (hourly) and V is the effective volume of that portion of the atmosphere contained within the Basin cold-air pool (hereafter referred to as the pollution layer). The daily change in CH_4 mole fraction is converted to density by assuming an atmospheric pressure of 850 mb and a temperature of 273.15 K (0°C) for each event. These conditions were selected as mean representative values of the boundary-layer conditions based on surface observations. The BEE approach is calculated on a ~1.33 km grid across the Basin, over all grid points n. The effective total volume V of the pollution layer is calculated by multiplying the surface area A_i (m^2) at each grid point index i by the depth in meters above ground level of the pollution layer at each grid point (Δz_i), and then summing these values over all Basin grid points contained within the pollution layer. The total depth ($\Delta z_i = z_i^t - z_i^g$) at each grid point of the pollution layer is defined as the difference between the elevation above sea level of the top of the cold-air pool z_i^t, and the elevation above sea level of the ground surface z_i^g. The values of z_i^g are defined by topographical fields (**Figure 1b**) from the National Land Cover Database (NLCD). The top of the pollution layer z_i^t is assumed to be a constant height above sea level at all grid points (a flat 'lid' intersecting the topography) based on findings of previous observational and modeling studies of cold-air pools and is determined by ceilometer imagery (Section 2.4). Thus, Δz_i is greatest at low elevation locations within the Basin and decreases with increasing surface elevation.

The BEE approach is only valid when limited mixing or dilution occurs between the overlying atmosphere and the pollution layer and when the spatial observation locations utilized are sufficiently representative of the surrounding boundary-layer. In these situations, a constant emission rate (E) into the pollution layer volume (V) within the Basin would increase the density (ρ) of CH_4 within the volume at a proportional rate over time (t). Ceilometer mixing height (h) data is used in this study (Section 2.4) to estimate the height above sea level of the capping inversion (flat 'lid' of the cold-air pool). Thus, in practice Δz_i is computed as the difference in elevation (above sea level) between the underlying topography and the height of the pollution layer lid estimated from the ceilometer. The daily rates of CH_4 increase are calculated using linear regression on CH_4 observations from three observational sites (Section 2.3). The regression fit is calculated using the daily average afternoon CH_4 between the hours of 2000 and 2300 UTC, because at this time of day surface observations are most representative of the polluted air column within the boundary-layer.

The last step in the BEE approach is to proportionally allocate the derived rates of CH_4 increase at each observation location to the Basin total by weighting the stations spatially using HRRR-STILT transport simulations (Section 2.7).

2.3 Methane surface observations

High-frequency CH_4, CO_2, and water vapor (H_2O) observations have been collected by the Utah Atmospheric Trace gas and Air Quality (U-ATAQ) lab at the University of Utah at three sites within the Uintah Basin since January 2015: Fruitland (FRU), Roosevelt (ROO), and Horsepool (HPL) (**Figure 1a**). A fourth site, Castle Peak (CSP), operated for a more limited time, from November 2015 to May 2016. Detailed information on the CH_4 instrumentation methodology, including calibration standards for all observations used in this study are given in Bares et al. (2019). The CH_4 (uncertainty σ = ±4.5 ppb), CO_2 (uncertainty σ = ±0.37 ppm), and H_2O (uncertainty σ = ±61 ppm) mole fraction measurements were collected as 10 second integrations of 1 Hz scans using a Los Gatos Research (LGR) Ultraportable Greenhouse Gas Analyzer (model 907–0011, Los Gatos Research Inc, San Jose, Ca.). The uncertainty is determined by utilizing calibration tanks that are periodically remeasured relative to WMO-calibrated tanks (Bares et al. 2019). H_2O mole fractions were calibrated using a Li-Cor LI-610 portable dew point generator (LI-COR, Lincoln NE) while corrections for water vapor on CO_2 and CH_4 were made mathematically by the LGR and validated in laboratory testing. CO_2 and CH_4 calibrations were performed every 3 hours using 3 compressed air tanks in sequence with known atmospheric mole fractions of CH_4 and CO_2 tertiary to the WMO scales. To account for instrumentation drift, we interpolated measurements of calibration gases during sampling periods and applied ordinary least squares regression to yield correction coefficients for each data point. The historic and real-time observations can be viewed at http://air.utah.edu.

These four observation sites are diverse in terms of location, surrounding topography, and ONG infrastructure (**Figure 1a** and **b**). Gas wells are generally confined to the southern and eastern portions of the Basin, while oil wells are located in the western and northern

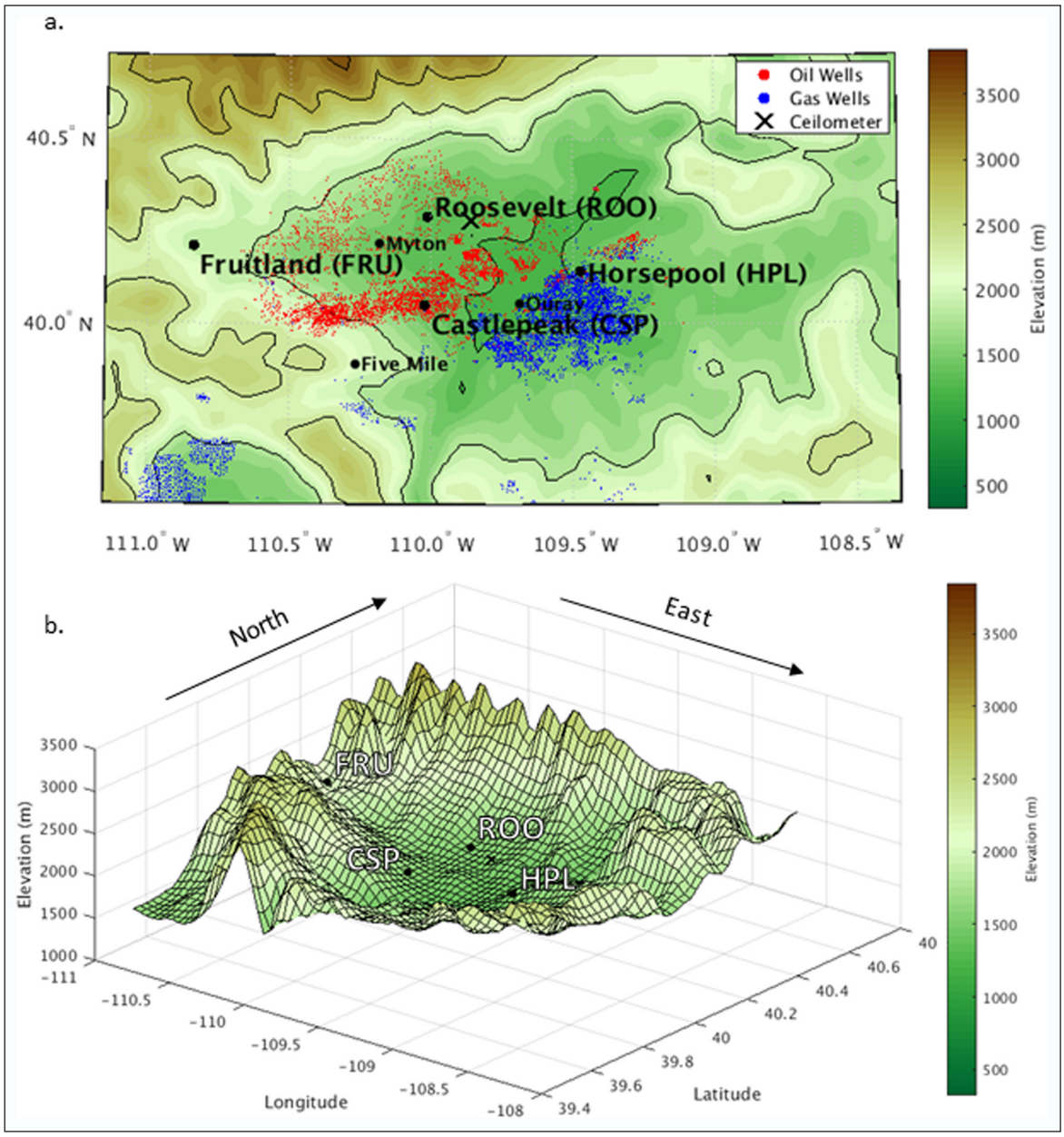

Figure 1: Uintah Basin terrain maps. (a) Elevation map (m) of the Uintah Basin showing the location of the Fruitland (FRU), Roosevelt (ROO), Horsepool (HPL), and Castle Peak (CSP) methane observing sites. Three other sites used for meteorological analysis are shown as well (Myton, Ouray, and Five Mile). Red dots indicate the location of active and producing oil wells and blue dots represent active and producing gas wells. The black "X" indicates the location of the ceilometer utilized in this study. **(b)** 3-D terrain map of the Uintah Basin showing elevation (m) relative to longitude and latitude. The location of FRU, ROO, CSP, and HPL are shown as black dots with corresponding identifiers and the location of the ceilometer is indicated by a black 'X'. DOI: https://doi.org/10.1525/elementa.362.f1

portions. The natural gas wells in the area to the south of HPL are densely situated, similar to the area of oil wells surrounding CSP (**Figure 1a**). ROO (1586 m elevation) is located within a broad area with a lower density of oil wells north of CSP, in the northwestern portion of the Basin. CSP (1605 m elevation) is centrally-located in the dense oil well production/extraction region in the western part of the Basin, while HPL (1569 m elevation) is situated at the north end of extensive gas well facilities near the bottom of the Basin. In contrast, FRU, located to the west, is elevated relative to the other three sites (2022 m) and generally upwind of the Basin. This makes FRU a favorable site for observing background levels of CH_4 (Foster et al. 2017).

The daily variations in CH_4 at the three low-elevation locations were used to estimate emission rates into the Basin volume. Only CH_4 observations between 2000 and 2300 UTC (1300 and 1600 LST) were used to calculate average daily afternoon CH_4 at each site. The rates of change over multiple days were then used to calculate daily increases in CH_4 at each site. The afternoon periods between 2000 and 2300 UTC were used in the analyses because afternoon mixing redistributes pollutants relatively uniformly with height throughout ~75% of the depth of the

pollution layer during this time of the day (Oltmans et al. 2016; Schnell et al. 2016). In contrast, stable to very stable near-surface inversions often exist during the nighttime, morning, and evening, and the observed surface CH_4 mole fractions at these times are not representative of values throughout the boundary layer, with large variations observed with height.

2.4 Ceilometer data and estimation of afternoon mixed-layer depth

Estimating afternoon mixed layer depth (h), and subsequently the depth of polluted air at each grid point in the Basin (Δz_i), is a crucial part of estimating CH_4 emission rates using the BEE methodology (Eq. 1). No operational rawinsondes are available in the Uintah Basin to determine profiles of temperature, stability, and h. Instead, to determine h, Vaisala CL-31 ceilometer data from Mesowest (Horel et al. 2002) at an elevation of 1,540 m within the Basin, approximately 10 km to the east of ROO (**Figure 1a**), was used. Many techniques, all with limitations, exist in the literature for determining h from ceilometers (Kotthaus et al. 2016). Best practice backscatter processing techniques have been used and developed at the University of Utah in relation to cold-air pool events (Neemann et al. 2015; Young and Whiteman 2015) and used to inform our methodology.

Our approach for this study uses visual mixed-layer height estimation during the afternoon between 2000 and 2300 UTC (when vertical mixing is highest), following the techniques utilized by Foster et al. (2017). Automated algorithms for processing ceilometer data can be adopted for longer periods (Sahoo et al. 1988), since visual identification of vertical gradients in ceilometer backscatter are too time prohibitive for those applications. This automated process can be used to identify gradients and therefore layers in the ceilometer images, as seen in **Figure 2**. The multilayering of ceilometer backscatter during prolonged cold-air pools in the Uintah Basin, however, makes it difficult

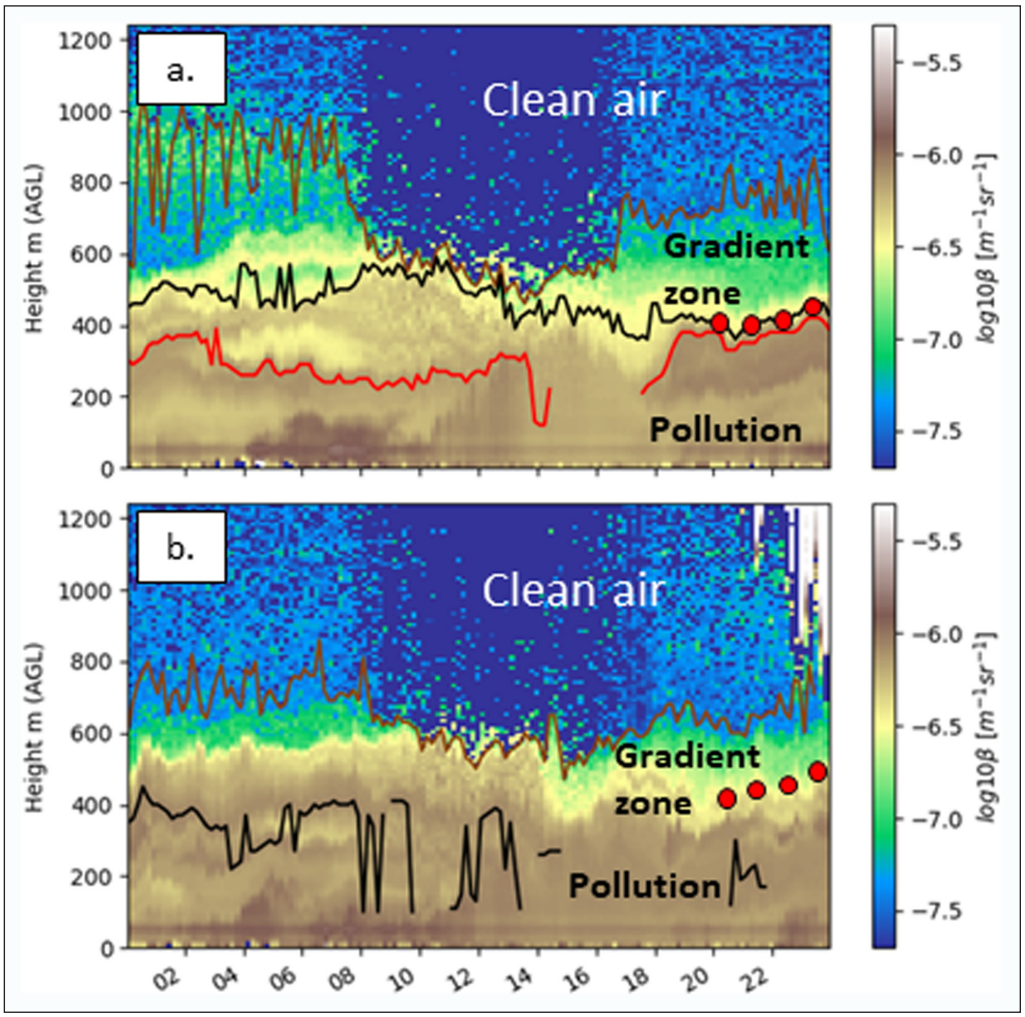

Figure 2: Ceilometer backscatter imagery and pollution layer depth estimates. Example ceilometer backscatter imagery from **(a)** 00 UTC 4 December 2015–00 UTC 5 December 2015 and **(b)** 00 UTC 3 January 2016–00 UTC 4 January 2016. The clean air, gradient zone, and polluted air are denoted. The red circles represent the visually estimated pollution depth determined between 2000 and 2300 UTC. The average values of these estimates are provided below (a) and (b). The brown and black lines indicate automated algorithm estimates of the height of the pollution layer depth used in the daily height estimate calculations and the red line indicates a shallower embedded pollution layer. DOI: https://doi.org/10.1525/elementa.362.f2

to distinguish residual layers aloft from primary ground-based mixed layers (our interest in this study). In this study visual identification of well-mixed surface layers, characterized by relatively homogenous vertical profiles in ceilometer backscatter during the afternoon, was found to be most effective approach, since the human eye can often see and analyze structures in the imagery that automated techniques miss. Therefore, the visual technique was adopted here, where the ceilometer time series is short enough for manual visual processing to be carried out.

Vertical profiles collected using rawinsondes and tethersondes during multiple wintertime cold-air pools in past years within the Uintah Basin, along with numerical model simulations, show that daytime heating results in *h* generally ranging between 250–500 m in depth in the lower portions of the Basin with a strong gradient in pollutants near the top of the inversion layer (e.g., Neemann et al. 2015; Schnell et al. 2016; Oltmans et al. 2016). Within this mixed-layer, nearly constant potential temperature and pollutant levels are observed. A strong capping temperature inversion typically exists above this layer, with a sharp gradient occurring (over a depth between 50–150 m) in pollution between the polluted air below and the clean air above. The main source of uncertainty in the techniques presented in this paper is error in the depth of the pollution layer used to constrain the 'top' of the basin volume calculation, which is estimated using ceilometer backscatter profiles. The afternoon mixed-layer depth, *h*, from the ceilometer was used to estimate the fixed vertical height above sea level of the pollution layer capping 'lid' across the Basin, or z_i^f as described in Section 2.2. The estimates for *h* were manually made from analyzing clear (non-cloudy) backscatter data from ceilometer data between 2000 and 2300 UTC, when solar heating of the land surface results in the highest vertical mixing (**Figure 2**). The afternoon *h* value was then used as the upper top bound on the volumetric calculation for CH_4 basin-wide build-up (Section 2.2). The mean estimated *h* are shown by red circles in **Figure 2**, while the mean afternoon *h* values are listed in **Table 1**.

Table 1: Afternoon (2000–2300 MST) ceilometer-derived boundary layer height (*h*) estimation for each day during Event A and Event B. DOI: https://doi.org/10.1525/elementa.362.t1

Event A		Event B	
Date	***h* (m)**	**Date**	***h* (m)**
29 Nov.	500	1 Jan.	475
30 Nov.	500	2 Jan.	400
1 Dec.	400	3 Jan.	475
2 Dec.	380	4 Jan.	450
3 Dec.	370	5 Jan.	400
4 Dec.	430	6 Jan.	350
5 Dec.	400		
Average	425		425
Range	375–475		375–475

2.5 Uncertainty analysis

We estimated uncertainty in our analysis by accounting for the following: (1) uncertainty in CH_4 tendency (calculated using a bootstrapping technique); and (2) uncertainty in mixed-layer height (estimated by visually examining the ceilometer backscatter imagery). To calculate the uncertainty in the linear regression of average afternoon CH_4 mole fractions, a bootstrapping technique was utilized. 10,000 bootstrapped samples were pulled from the time series of average afternoon CH_4 and the standard error of the population of the resulting slopes was calculated. To account for the inherent uncertainty in the Δz_i estimated from ceilometer *h* estimates for the BEE calculation, we calculate Δz_i with an estimated +/− 50 m error for each of the two events. This value was determined based on our assumed uncertainty in visually estimating the boundary layer heights from ceilometer data within a range of 100 m. For this study, mostly clear skies were noted, so their influence on boundary layer height estimation was minimal. During infrequent cloudy periods, when low clouds can obscure the ceilometer retrievals, the most recent clear sky available ceilometer pollution depth image was used to estimate the mixing height. The CH_4 tendency uncertainty and the mixing height uncertainty errors were then appropriately propagated to the final CH_4 emission estimate through the methods outlined in Taylor (1982) for propagating uncertainty in a function of several variables, which in this case are Δz_i and $\Delta\rho$.

2.6 Atmospheric transport model simulated footprints for measurement sites

Atmospheric simulations elucidating source regions for each of the measurement sites were conducted using the Stochastic Time-Inverted Lagrangian Transport (STILT) model (Lin et al. 2003), driven by meteorological wind fields from the High-Resolution Rapid Refresh (HRRR) model analyses archived by NOAA Air Resources Laboratory. These HRRR-STILT simulations were run for three periods: two cold-air pool case studies discussed in Section 2.6 that occurred between 28 November 2015 – December 2015 and 1–6 January 2016 as well as a comparison non-cold air pool period between 1–7 September 2015. The purpose of the two cold-air pool HRRR-STILT simulations were to provide output for determining the relative weighting factor applied to each of the 3 observation locations in the Basin, when applying the BEE approach (Section 2.2).

The operational HRRR model (https://rapidrefresh.noaa.gov/) is run over the contiguous U.S. at 3 km resolution and includes assimilation of radar observations (Benjamin et al. 2016). The wind fields from the HRRR model are used within STILT, a time-reversed Lagrangian particle dispersion model (Lin et al. 2003; Nehrkorn et al. 2010), to drive backward simulations of air parcel trajectories. An ensemble of air parcels are released from the measurement sites ("receptors") at each specified time, and the air parcels trace out the source regions (Lin et al. 2003). More details on the HRRR-STILT methodology and model parameters as well as a comparison between meteorological model simulation mixing heights and ceilometer data

are provided in Foster et al. (2017). The model simulations generally agreed with ceilometer estimates during a springtime period which included nocturnal cold-air pools in Foster et al. (2017). While weather models are known to have difficulty in simulating wintertime cold-air pools and generally overestimate vertical and horizontal transport (Neemann et al. 2015; Tran et al. 2018), no rigorous study has been conducted on the accuracy of the HRRR model in the Uintah Basin in wintertime. Qualitative evaluation of HRRR model output indicated that temperature inversions from the simulations conducted herein yielded modest errors and biases in the height and strength of these inversion layers. Future work will assess the degree to which the HRRR model errors may impact meteorological transport during wintertime cold-air pools. For this study, a crude HRRR model estimation of the source regions from which CH_4 emissions observed each of the receptor sites was deemed sufficient, as the BEE approach only utilizes HRRR-STILT model output for determining the relative weighting factor applied of each of the 3 observation locations in the Basin (Section 3.2). The 1–7 September 2015 simulation was run only to highlight the difference in parcel trajectories between the wintertime stagnant conditions used within the BEE methodology and typical atmospheric transport during warmer times of the year.

STILT-produced 'footprints,' which represent the upwind contribution of each grid cell in the source region on CH_4 mole fractions observed at the receptor (Lin et al., 2003), help determine the spatial extent to which each station is representative of the area surrounding it, as well as to provide confidence that trajectories remain primarily within the Basin during cold-air pool events. To help quantify these features, backward trajectories and footprints are simulated for air parcels at each of the sites during the stable wintertime cold-air pools case studies (Sections 2.7). The area covered by each measurement site's footprint is indicative of how well the site represents the entire Basin for the linear regression analysis discussed in Section 2.3, so the estimated emission rates are weighted based on the area each site's footprint covers. Each event's average footprint (hourly afternoon footprint averaged over the duration of the event) was spatially multiplied by the density of gas wells as seen in **Figure 1a** and this product was summed over the entire Basin to calculate the footprint-weighted well number (**Table 2**). The footprint-weighted well number is an indication of the extent to which each station is representative of overall emissions within the Basin, under the assumption that emissions take place at the well locations. If a station has a more spatially expansive and higher footprint value that coincides with areas of densely situated wells, then its footprint-weighted well number will be higher. This method seeks to weigh more heavily in the final BEE analysis of CH_4 emission rates in the Basin those observing stations that are most representative of Basin emission sources as quantified through the footprint-weighted well number. As shown in **Table 2**, the CSP and HPL observation locations have over twice the footprint-weighted well numbers due to the large emission sources surrounding these centrally-located stations in the Basin.

2.7 2015–2016 study period and meteorological case study selection

The BEE methodology was applied to the winter period of 2015–2016 to estimate CH_4 emissions from the Uintah Basin. This winter was specifically chosen since CSP was operational during this time period, and therefore measurements are available for all four sites within the Basin: FRU, CSP, ROO, and HPL (**Figure 1a** and **b**).

In order to estimate cold-air pool strength, data from three Mesowest meteorological sites (Horel et al. 2002) were utilized (**Figure 3**). Ouray (elevation 1411 m) is located in the lowest portion of the Basin, whereas Myton (elevation 1609 m) is located at a slightly higher elevation on the western edge of the lowest portion of the Basin. Five Mile (elevation 2280 m) is located on the southern slope of the Basin, and the difference in temperature between this station and the lower elevation stations provides a proxy of the cold-air pool strength, as no rawinsondes were available during the periods of study (Whiteman et al. 2014).

Table 2: CH_4 emission rate data for each station and event, as labeled. CH_4 tendency (ppb day^{-1}, ceilometer boundary-layer h estimates, which are used to estimate Δz_i (m) at each grid point, emissions rates (kg CH_4 hr^{-1}), footprint-weighted well number, and the final basin-wide emissions rates are shown (kg CH_4 hr^{-1}). DOI: https://doi.org/10.1525/elementa.362.t2

	Tendency (ppb day^{-1})	h (m)	Emission Rate (kg CH_4 hr^{-1})	Footprint-Weighted Well Number	Weighted Mean (kg CH_4 hr^{-1})
HPL A	332 +/– 24	425 +/– 50	42.32 +/– 9.66	5.12	
ROO A	286 +/– 13	425 +/– 50	36.43 +/– 8.06	2.05	
CSP A	389 +/– 32	425 +/– 50	49.57 +/– 11.48	5.71	
TOTAL					44.60 +/– 10.29
HPL B	954 +/– 108	425 +/– 50	122.15 +/– 29.80	6.50	
ROO B	451 +/– 47	425 +/– 50	57.46 +/– 13.80	2.07	
CSP B	497 +/– 129	425 +/– 50	63.28 +/– 21.39	6.18	
TOTAL					61.82 +/– 19.76

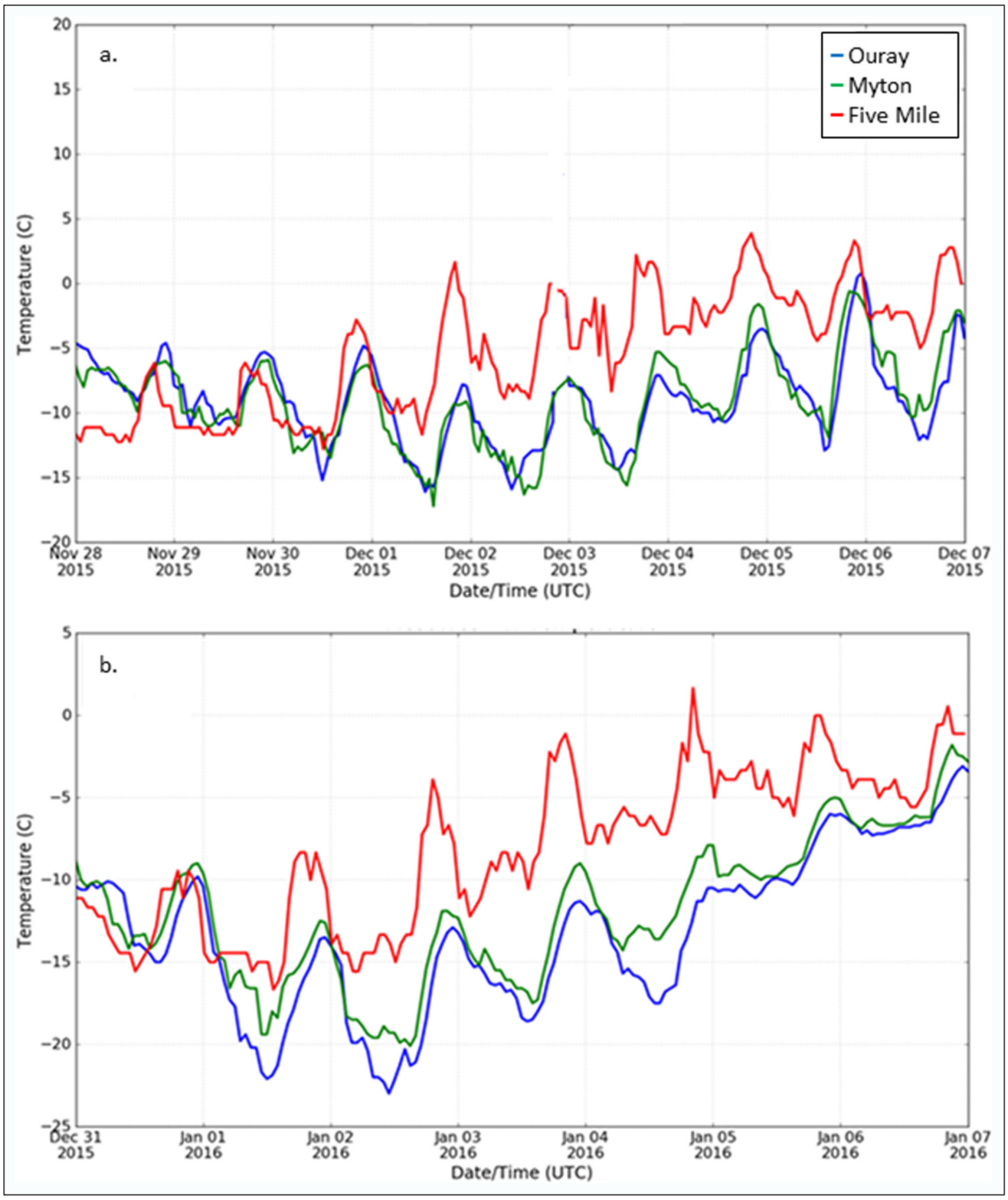

Figure 3: Time series of 2-m air temperature at supplementary stations. Time series of 2-m air temperature from Mesowest at station Ouray (blue line, elevation 1411 m), station Myton (green line, elevation 1411 m) and station Five Mile (red line, elevation 2280 m) for **(a)** 28 November – 6 December 2015. **(b)** 31 December 2015–6 January 2016. DOI: https://doi.org/10.1525/elementa.362.f3

The case studies were chosen based on meteorological cold-air pool conditions that allowed the Basin's boundary-layer to be considered a quasi-closed system of known volume *V*, and that allowed for the use of ceilometer in estimating mid-afternoon boundary-layer height, in order to apply the BEE methodology (Eq. 1; Section 2.2). For this situation to occur, the following conditions needed to be met within the Basin: generally clear skies and absence of precipitation (to minimize ceilometer interference), and undisturbed large-scale synoptic flow. In the presence of strong winds or precipitation, CH_4 mole fractions would not increase as rapidly within the Basin volume due to mixing and dilution of the polluted boundary-layer with cleaner air from aloft (Neemann et al. 2015). Conditions of prolonged stagnation and CH_4 build-up ideal for investigation with the BEE occurred only twice during the 2015–2016 winter period (**Figure 4**). Due to these criteria a number of the strongest cold-air pools, which are often cloud-filled and therefore show increased backscatter in ceilometer imagery, are removed from further consideration in this study.

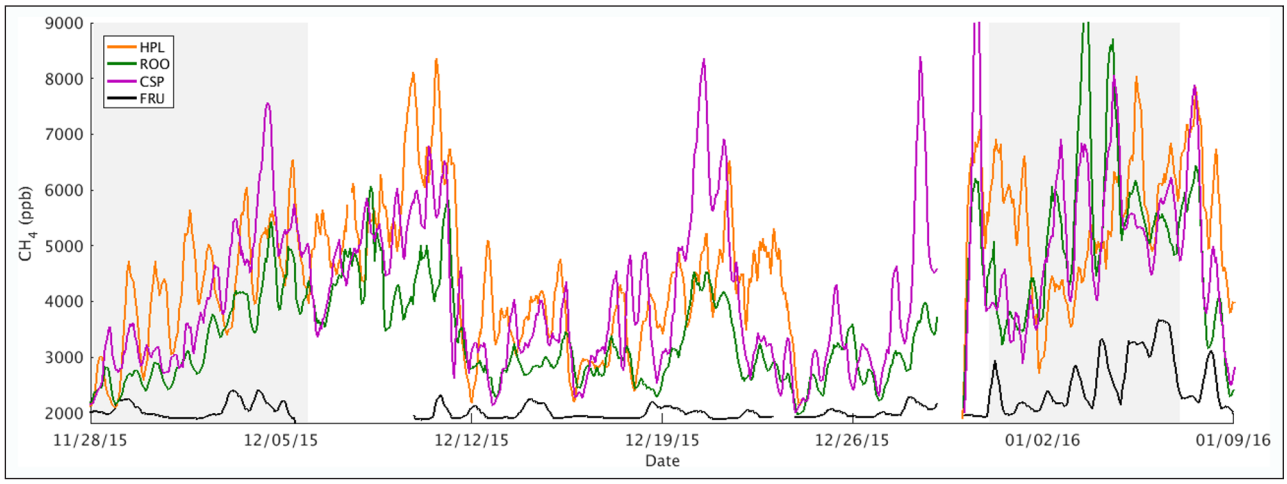

Figure 4: Key methane observations. Time series of CH_4 (ppb) between 28 November 2015 and 9 January 2016 at the four observation locations within the Uintah Basin (HPL, orange line; ROO, green line; CSP, purple line; FRU, black line). The two shaded periods (28 November 2015–6 December 2015 and 1–6 January 2016) represent two cold-air pool periods (Events A and B, respectively) chosen for this study where significant clouds, mixing or precipitation did not occur. DOI: https://doi.org/10.1525/elementa.362.f4

The first case study (hereafter referred to as "Event A") began on 28 November 2015 and ended 6 December 2015 (**Figure 4**). Between 28 November – 5 December 2015, generally clear skies and a shallow polluted boundary-layer with depths between 400–500 m were observed (**Figure 2a** and **Table 1**). A moderate vertical temperature inversion during this event is noted, with the elevated Five Mile meteorological site observing 2-m air temperature 5–10°C warmer than in the bottom of the Basin (**Figure 3a**). The steady daily increase in CH_4 ended on 6 December, when CH_4 dropped due to mixing into Basin volume from clouds (**Figure 4**). Toward the end of Event A, CH_4 mole fractions at FRU were also elevated, suggesting the height of the capping inversion became elevated enough that the Basin emissions from upslope flows began to impact it, as well.

The second case study (hereafter referred to as "Event B") began on 1 January 2016 and ended 6 January 2016, spanning 5 days (**Figure 4**). Event B made up a portion of the longest duration cold-air pool of the 2015–2016 winter, which occurred between 24 December 2015–10 January 2016 (**Figure 5**). However, clouds, precipitation, and winds precluded analysis of CH_4 build-up during other periods. A moderate vertical temperature inversion during this event is noted, with the elevated Five Mile meteorological site observing 2-m air temperature 5–10°C warmer than in the bottom of the Basin (**Figure 3b**). However, in the portion of the Basin near HPL, the combination of deeper snow cover, surface fog, and high clouds all limited insolation and resulted in a local cold pool. This is shown by the temperatures being ~2°C cooler at the weather station near HPL than the other low-elevation stations on the western side of the Basin (**Figure 3b**). This local cold-air pool remained stable even during the afternoon, and we hypothesize that the boundary-layer at HPL did not mix out in the afternoon above ~250 m, as indicated by the lack of typical diurnal variations in CH_4 during this period. Because of this, HPL was excluded from the CH_4 build-up estimates for event B.

3 Results and Discussion

3.1 Daily increases in methane at observing sites

During events A and B, the daily estimates in observed CH_4 mole fractions at the low-elevation locations in the Basin approximated by the linear regression fits to observed CH_4 time series during afternoon mixed boundary-layers ranged between 280–500 ppb day^{-1} (**Figure 5**). For event A, the three sites in the Basin showed increases in daily CH_4 levels of ~280–380 ppb day^{-1} (**Figure 5**). For Event B, the CH_4 increases per day are slightly higher than Event A, ~450–500 ppb day^{-1}. HPL and CSP observed generally higher estimated daily increases in observed CH_4 compared to ROO, which is consistent with expectations of higher local emissions due to the higher density of ONG industry in the vicinity of HPL and CSP.

3.2 Spatially allocating methane observations for BEE

The amount of horizontal transport beneath the strong capping lid in cold-air pools, represented by the shape and extent of the meteorological footprints (**Figure 6**), impacts the calculation of basin-scale emission rate. The amount of horizontal transport may vary somewhat from episode to episode and certainly between different sub-regions within the Basin. Over the duration of these episodes, average footprints suggest that air parcel back trajectories remain primarily within the Basin (**Figure 6**), which is what would be expected given the highly stable conditions. Footprint values are confined to the Basin, and the gradients tend to follow the model topography. These footprints represent the source areas of the Basin that most heavily influence CH_4 mole fractions observed at the measurement sites, so when the footprints coincide with underlying emissions sources (e.g., wells), the

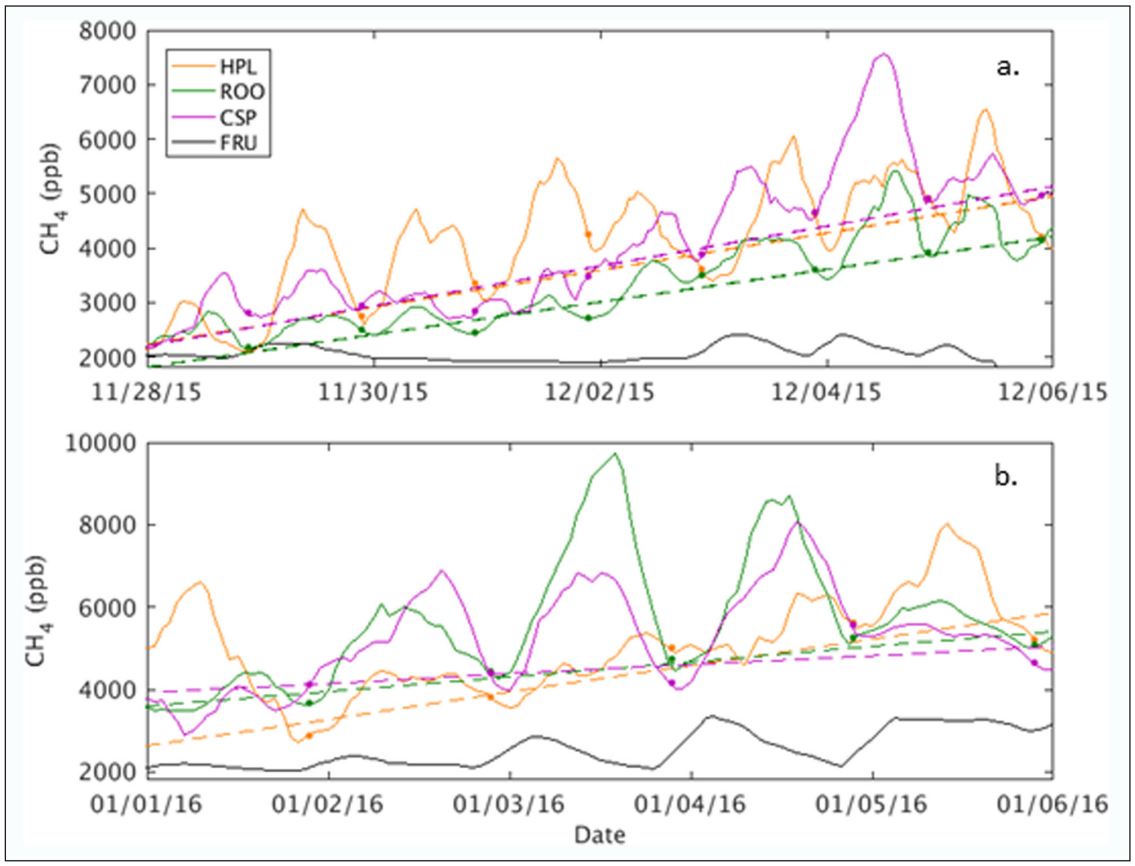

Figure 5: Daily methane tendency estimations. (a) Time series of hourly average CH_4 mole fractions (ppb) at HPL (orange), ROO (green), CSP (magenta), and FRU (black) from 11 November – 6 December 2015 (Event A). **(b)** Time series of hourly average CH_4 at the same sites from 1–6 January 2016 (Event B). Daily averaged afternoon (2000 to 2300 UTC) CH_4 levels are plotted as dots and the linear regression fits to the time series of daily minimum CH_4 are plotted as dashed lines, with colors corresponding to the observation locations shown in the legend. DOI: https://doi.org/10.1525/elementa.362.f5

sites are weighted more heavily, such as in the case of HPL (**Figure 6b** and **e**) and CSP (**Figure 6a** and **d**). ROO is weighted less than the other two sites due to lower density of wells surrounding it and also due to the fact that its simulated footprints are more confined to the northwestern portion of the Basin (**Figure 6c** and **f**).

3.3 Comparison of spatial footprints for a non-cold-air pool episode

The average footprints at CSP, HPL, and ROO for a period in September are shown in **Figure 7** to contrast against the wintertime cold-air pool conditions shown in **Figure 6**. In the wintertime cold-air pool cases, the footprint contributions at CSP, HPL and ROO are focused within the Basin (**Figure 6**), illustrating that air parcel back trajectories remain largely trapped within the stable Basin cold-air pool. However, in the September case (**Figure 7**), footprint contributions from within the Basin are much lower, with notable footprint contributions from locales to the southwest, outside of the Basin, reflecting increased transport from more distant regions during warmer September conditions. Clearly, the BEE approach would not be appropriate to be applied during non-cold-air pool situations such as those observed here, as no effective Basin volume could be calculated that contained air parcel trajectories.

3.4 Estimated Basin-wide methane emission rates

Results of the BEE technique as applied to Events A and B are summarized in **Table 2**. The emission rate estimated using event A was 44.60 +/– 9.66 × 10^3 kg CH_4 hr^{-1} and excluding the results from HPL, the estimated emission rate for event B was 61.82 +/– 19.76 × 10^3 kg CH_4 hr^{-1}.

Examining the emission rates estimated using each site separately shows that variations are present within the Basin even during cold-air pool conditions (**Table 2**). CH_4 tendencies were overall lower for Event A, resulting in lower emission rates due to the proportionality of these variables and similar estimated h (Eq. 1). However, primarily due to the local cold pool (Section 2.6), the CH_4 emission rate calculated using the CH_4 tendencies observed at HPL during Event B was twice that calculated at ROO and CSP for the same event (**Table 2**). The minor differences in CH_4 tendency between the three sites within each event suggest a simpler methodology could provide a first-order estimate of CH_4 emissions using only one site, without the need to weight each site relative to the footprints and well density. However, these small variations suggest that signals of heterogeneous emissions throughout the Basin as imprinted upon the CH_4 mole fractions are not completely mixed away within winter time cold-air pool conditions.

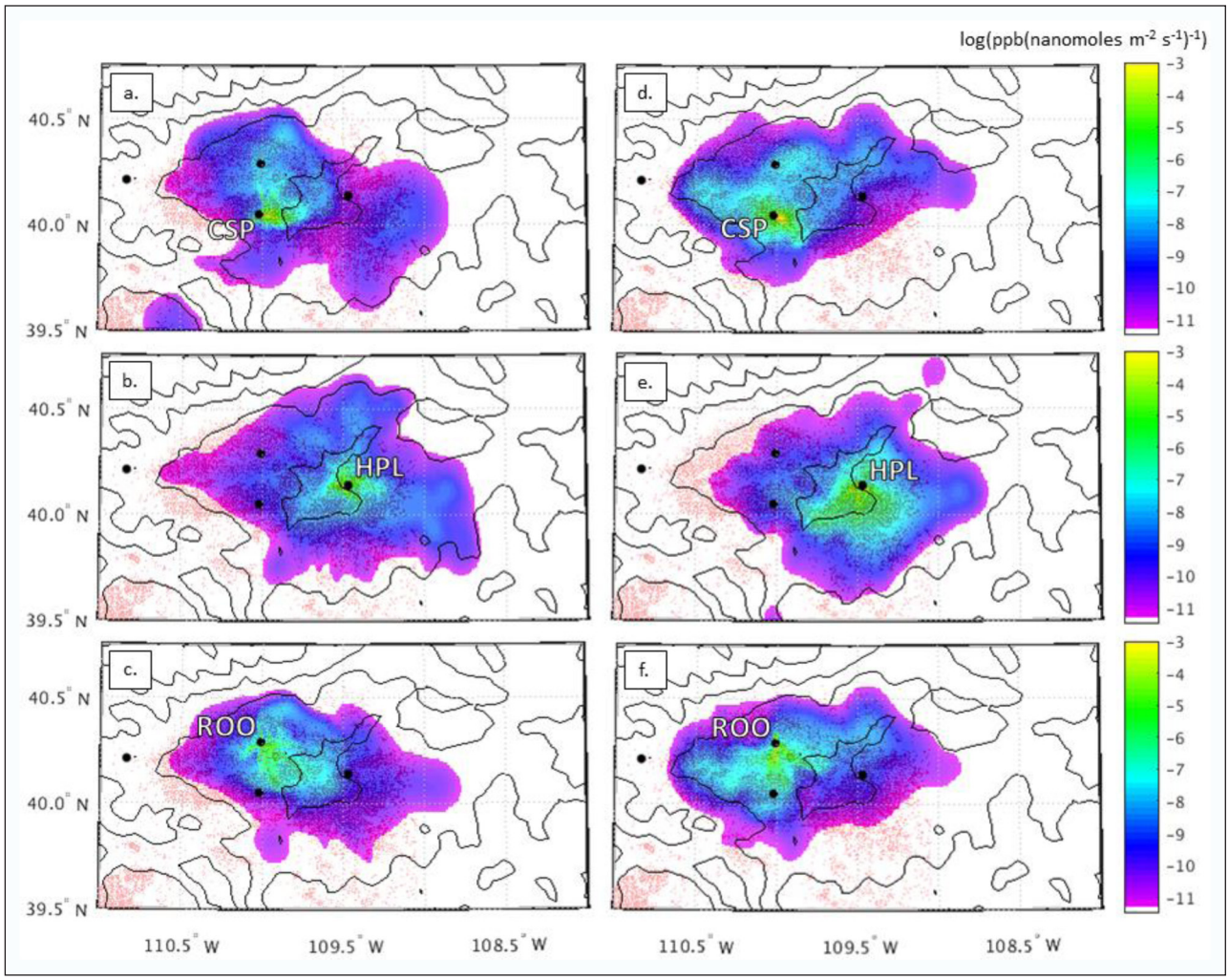

Figure 6: Average wintertime STILT footprints. Map of the Uintah Basin showing the average daytime footprint log(ppb(nanomoles m^{-2} s^{-1})$^{-1}$) over the duration of Event A (28 November 2015 to 6 December 2015) for **(a)** Castle Peak, **(b)** Horsepool, and **(c)** Roosevelt and Event B (1 January 2016 to 6 January 2016) for **(d)** Castle Peak, **(e)** Horsepool, and **(f)** Roosevelt. Underlaid on each map in black dots are the locations of oil and gas wells. DOI: https://doi.org/10.1525/elementa.362.f6

The estimated CH_4 tendencies computed in this study are consistent with past methods used for estimating Uintah Basin emission rates. Karion et al. (2013) estimated the emission rate for the region of natural gas wells in the southeast portion of the Basin to be 56×10^3 kg CH_4 hr^{-1} using a single research flight and a mass balance approach in February 2012. While Karion et al. (2013) found no evidence to suggest this day was substantively unique to any other, their result could be an under- or overestimation of total, annual basin-wide emissions as a result. This emission rate was spread over the entire Basin by Ahmadov et al. (2015) to create an inventory of CH_4 emissions according to the locations of ONG wells. Due to the methodology of applying an emission estimate for one portion of the Basin over its entirety, the Ahmadov methodology is more than likely an underestimation. Foster et al. (2017) compared the Ahmadov inventory estimate to 2015 and 2016 CH_4 observational data using STILT to simulate CH_4 mole fractions based on available emission inventories and found agreement with the Ahmadov et al. (2015) inventory at HPL and CSP, albeit slightly underestimated. However, both the top-down (Ahmadov) and bottom-up (EPA; Maasakers et al. 2016) inventories substantively underestimated emissions in the area around ROO, suggesting critical uncertainty in emissions from this region. Event A's estimate is roughly 80% of the Karion et al. (2013) estimate, while Event B is around 110% of the Karion estimate, and the proximity of these estimates support the validity of the methodology presented in this study. Differences in emission rates between the events in this study are possibly both the result of the simplified methodology not accounting for intricacies in the transport and mixing of emissions within the Basin or different amounts of mixing with the free-troposphere between events, as well as the duration of time (~one month) separating the two cold-air pool episodes. A possible but unverified explanation for the difference in estimated emission rates between events could be the timing of maintenance activities, such as manual liquid unloadings or venting (Burnham et al. 2012; Schwietzke et al. 2017).

The results of this study provide additional support for previous studies that suggest the recent EPA inventory

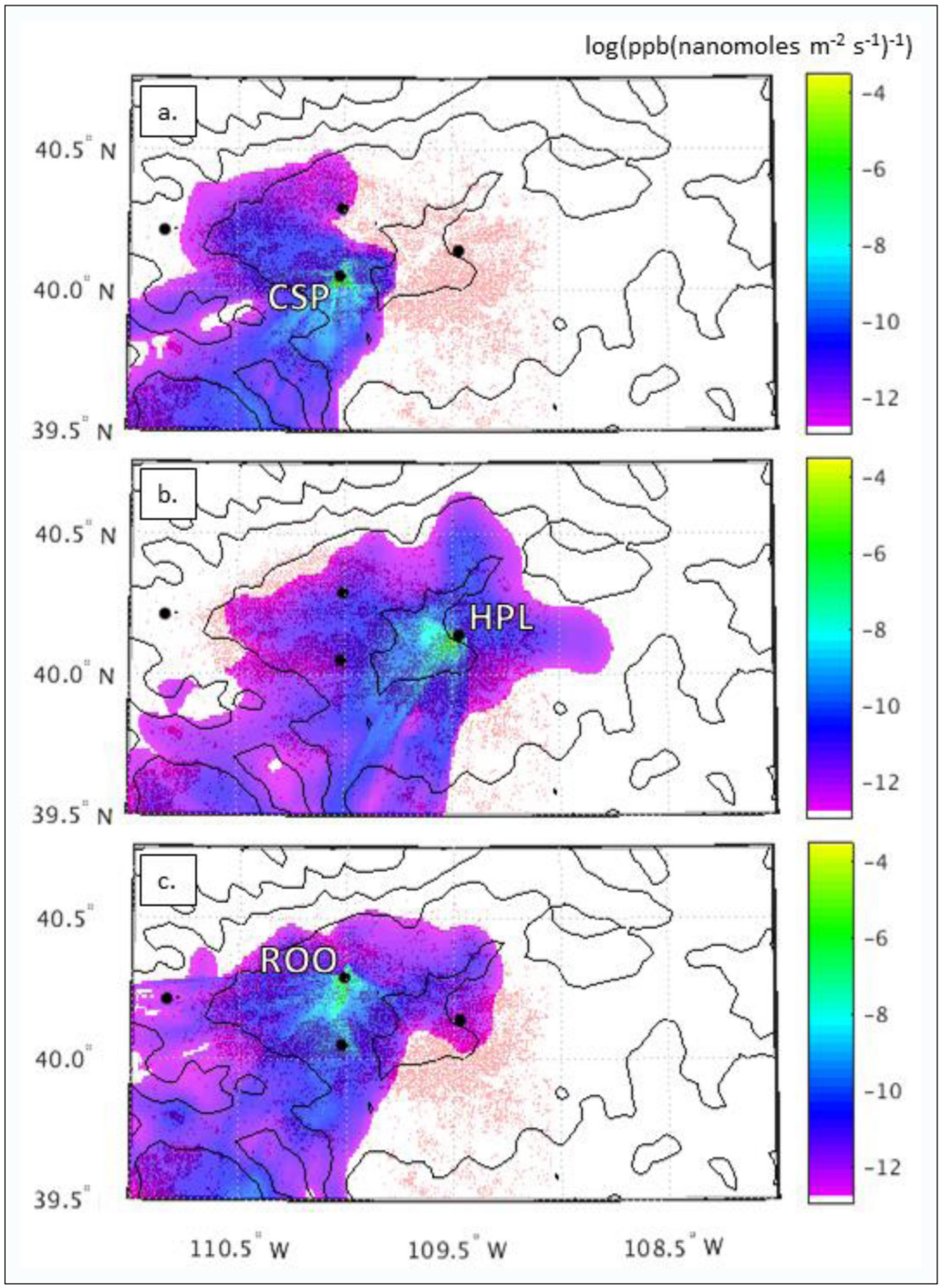

Figure 7: Average September STILT footprints. Map of the Uintah Basin showing the average footprint log(ppb(nanomoles m^{-2} s^{-1})$^{-1}$) from 1–7 September 2015 for **(a)** Castle Peak, **(b)** Horsepool, and **(c)** Roosevelt. Underlaid on each map in black dots are the locations of oil and gas wells. DOI: https://doi.org/10.1525/elementa.362.f7

underestimates CH_4 emissions in the Basin. The CH_4 emissions estimates for the two events presented in this paper are roughly 50–100% higher than the estimate from a gridded EPA inventory, 31.1 × 10^3 kg CH_4 hr^{-1} (Foster et al. 2017; Maasakkers et al. 2016), which is similar to the 60% discrepancy between aircraft-validated and EPA emission estimates found by Alvarez et al. (2018). Foster et al. (2017) found underestimations between reported CH_4 emissions in the northwestern portion the Basin based upon observations at ROO, and lesser underestimates near CSP and HPL, which the results of this study also support.

While the BEE approach is simple in theory, even in ideal conditions there are complicating factors and sources of error to be considered. These include but are not necessarily limited to: (1) assuming the ceilometer backscatter is a good proxy for the afternoon mixed-layer depth, (2) assuming that the pollution layer depth is uniform across the Basin, (3) unaccounted for dilution of the polluted boundary layer with clean air from lateral or vertical transport, and (4) insufficient representativeness of the three CH_4 observation locations to the larger Basin volume, given the stable conditions and limited horizontal mixing that occurs during wintertime in the Basin.

4 Summary and Future Work

The BEE technique was presented in this paper as a means for utilizing *in situ* CH_4 times series data, combined with known pollution layer depth and topography, to constrain total basin-wide emissions of CH_4 within the heavily developed ONG infrastructure of the Uintah Basin. The BEE approach yielded CH_4 emission rates from oil and natural gas infrastructure between $44.60 +/- 9.66 \times 10^3$ and $61.82 +/- 19.76 \times 10^3$ kg CH_4 hr^{-1}, which are similar to the estimates proposed by previous studies performed in the Uintah Basin, and greater than the gridded EPA inventory, whose emission rates of 31.1×10^3 kg CH_4 hr^{-1} underestimate emissions in the Basin (Foster et al. 2017). The BEE approach could likely be applicable to other developing ONG producing basins worldwide with similar meteorology and bowl-like topography. In the United States alone, several basins in the Western USA have increasing oil and natural gas production, where pollution from these industries may become a greater concern in the future (Mansfield and Hall 2018). While targeted aircraft campaigns can provide estimates of basin-scale emissions, they are too expensive to be undertaken frequently, and the mass-balance technique may encounter difficulties with budget closure in complex topography such as the Uintah Basin. In addition, aircraft campaigns only provide snapshots of emissions during limited flight times, mainly during the daytime, rather than temporally-representative observations, which don't reflect diurnal or long-term variations (Vaughn et al. 2018). Recent studies have indicated the need for temporally-representative CH_4 observations within ONG production regions so changes in leakage rates over time can be determined. It has been suggested that daytime emissions are higher than those at night, due to the processes associated with midday operations, such as manual liquid unloadings, so these studies are possibly observing higher-than-average emissions as a result of the time constraints (Schwietzke et al. 2017). Higher daytime activities related to manual unloadings have been documented in the HPL region of the Basin (Lyman and Shorthill 2013).

A strength of this study is the temporal integration and averaging inherent in the CH_4 buildup during the cold-air pool stagnation periods, which were 5–7 days in duration. In other words, a key advantage of BEE for calculating CH_4 build-up within a cold-air pool is the ability to integrate both daytime and nighttime emissions into the volume. However, an inherent limitation to estimating emissions during cold-air pool stagnation periods is that the results are potentially biased to represent the oil and natural gas production activities during these wintertime periods, which are often snow covered and cold, and could potentially be different than average or 'normal' activities over longer time scales in the Basin.

A noted strength of this study is that through an independent methodological approach we further validate the general findings of previous studies (Karion et al. 2013; Ahmadov et al. 2015; Foster et al. 2017) that leak rates of CH_4 in the Uintah Basin are among the highest in the US. We also find it noteworthy that despite the differences in analysis approaches (single aircraft flight, modeling and observational approaches) and analysis times (2012 for Karion et al. 2013, 2015–2016 for Foster et al. 2017 and this study) all yield similar leak rates of CH_4 in the Basin. The overall cross-study agreement likely adds additional validation to the findings of each study individually.

Another strength of this study is the relative consistency of estimated CH_4 emissions rates from all three spatially distinct observation locations. While the HRRR-STILT model was run for the entire episode to provide trajectory and footprint estimates (Foster et al. 2017) to provide relative weighting of the three lower-elevation observation locations, the HRRR-STILT model runs were not used in calculating the rates of CH_4 increase at HPL, CSP, or ROO individually. It should be noted that the stations are fairly uniform in observed afternoon CH_4 levels during both episodes (**Figure 5a** and **b**), and the HRRR-STILT derived spatial footprints of each of the three locations are relatively similar in horizontal extent (**Figure 6**).

Several potential limitations of the BEE approach as applied in this study could result in either overestimations or underestimations of basin-wide CH_4 emission rate. Due to the key assumption of limited vertical or lateral exchange with air outside the cold-air pool, the BEE results may be a lower bound for the potential CH_4 emissions from the Basin. If horizontal and vertical mass exchange are larger than assumed during these wintertime episodes, then the BEE approach could be underestimating emissions from the entire Basin. On the other hand, atmospheric models like HRRR-STILT could potentially overestimate vertical and horizontal transport within the cold-air pool, a known weakness in simulations of cold-air pools. If we were to assume smaller, more confined footprints, rather than the whole Basin, in calculating *V*, lower emissions estimates would result, since the emissions necessary to force the same daily increase in CH_4 within the smaller volume would be lower. Future analysis of more wintertime cases needs to be conducted to verify the validity of this result for more wintertime cold-air pools, which will become possible as the period of record of the unique CH_4 observations collected as part of this study lengthens.

The location of ONG wells, as well as production, processing, and distribution facilities, varies throughout the Basin, and it is likely that emission rates vary spatially and between different types of infrastructure (e.g., wells versus larger production facilities). In this study, observed CH_4 mole fractions are highest surrounding HPL and CSP, and lowest near ROO, which is generally reflected in lower average CH_4 observed at each site and assumed proportional to the density of oil and natural gas wells (Foster et al. 2017, **Figure 1a**). These differences are accounted for within the methodology; however, they are thought be real characteristics of each location since it is known that CH_4 emissions are heterogeneous throughout the Basin and local influences will still be seen even within cold-air pool conditions.

The simulated footprints during the cold-air pools (**Figure 6**) illustrate that much of CH_4 observed in each of the three observation locations within the Basin likely originated from the dominant production, processing, and distribution facilities in that portion of the Basin (**Figures 1** and **6**). Thus, near CSP, emissions from oil extraction/processing likely dominate, whereas near HPL, emissions from natural gas extraction/processing likely

are the most significant. However, during these long-duration stable layers, significant overlap between source regions is seen (**Figure 6**), complicating the potential for separating the analyses of contributions of different areas and sectors in the Basin at each observation location. Future work could look at shorter time periods to more effectively isolate emission sources at observation locations utilizing model trajectory analyses.

Methane emissions from ONG infrastructure contribute substantively to the global source of this potent greenhouse gas, and the number of producing and active ONG wells is continually changing in time. The reported activity data in emissions inventories may be out of date, and care needs to be taken with comparing observations from one time period with inventories developed during a different time period (Vaughn et al. 2018). Many studies have been performed to estimate the total emissions of CH_4 from areas where the ONG industry is prevalent, utilizing a variety of methodology and measuring platforms. The ongoing dataset of *in situ* CH_4 data available in the Uintah Basin beginning in 2015 affords the opportunity to examine CH_4 variability in an ONG region in new and unique ways. Utilizing CH_4 data from winter cold-air pool episodes to estimate emissions within the Uintah Basin proved viable when comparing results to previous studies in the same basin. Improvements could be made in terms of methodology, including analyzing more time periods as the dataset lengthens. Investigating each winter could provide a better understanding of how emissions relate to time-variable aspects of the industry. As data collection continues, it can inform changes in emissions from ONG regions such as the Uintah Basin using a simple method like BEE. Future work will be required to determine if variations in emission rates as a function of time of day, region, or ONG infrastructure type can be gleaned from the ongoing CH_4 observations in the Uintah Basin. The research presented here can be expanded upon by utilizing more events and improving the BEE methodology, either by using other methods to estimate boundary layer heights (soundings) or further partitioning the basin based on the siting characteristics of each station.

Data Accessibility Statement

The following data sources were used in this study:

- Real-time and historic CH_4 measurements from all sites presented in this study can be viewed at: http://air.utah.edu.
- Real-time and historic meteorological measurements from all sites presented in this study can be viewed at: https://mesowest.utah.edu/.
- Archived ceilometer imagery used in this study can be viewed at: http://meso1.chpc.utah.edu/ceilometer/URHSC/.
- More information regarding the archived Uintah Basin methane data can be found in the following publication:
  Title: The Utah urban carbon dioxide (UUCON) and Uintah Basin greenhouse gas networks: Instrumentation, data and measurement uncertainty.
  Authors: Bares, R., L. Mitchell, B. Fasoli, D. Bowling, D. Catherine, M. Garcia, B., Eng, J. Ehleringer, and J. C. Lin.
  Status: Published at https://doi.org/10.5194/essd-2018-148.

Acknowledgements

We thank Maria Garcia for providing the calibration tanks, Dr. David Bowling for providing a calibration facility, and Derek Mallia for help with the STILT simulations. Feedback on this work from Gannet Hallar is greatly appreciated.

Funding information

This study was performed with the support of NOAA Climate Program Office's Atmospheric Chemistry, Carbon Cycle, and Climate program, award #NA14OAR4310138 (PI: J. C. Lin).

Competing interests

The authors have no competing interests to declare.

Author contributions

- Contributed to conception and design: CSF, ETC, JCL
- Contributed to acquisition of data: SL, BF, RB, JCL
- Contributed to analysis and interpretation of data: CSF, ETC, JCL
- Drafted and/or revised the article: CSF, ETC, JDH, SL, BF, RB, JCL
- Approved the submitted version for publication: CSF, ETC, JDH, SL, BF, RB, JCL

References

Ahmadov, R, McKeen, S, Trainer, M, Banta, R, Brewer, A, Brown, S, Edwards, PM, De Gouw, JA, Frost, GJ, Gilman, J, Helmig, D, Johnson, B, Karion, A, Koss, A, Langford, A, Lerner, B, Olson, J, Oltmans, S, Peischl, J, Petron, G, Pichugina, Y, Roberts, JM, Ryerson, T, Schnell, R, Senff, C, Sweeney, C, Thompson, C, Veres, PR, Warneke, C, Wild, R, Williams, EJ, Yuan, B and **Zamora, R** 2015. Understanding high wintertime ozone pollution events in an oil- and natural gas-producing region of the western US. *Atmos. Chem. Phys* **15**: 411–429. DOI: https://doi.org/10.5194/acp-15-411-2015

Alvarez, RA, Zavala-Araiza, D, Lyon, DR, Allen, DT, Barkley, ZR, Brandt, AR, Davis, KJ, Herndon, SC, Jacob, DJ, Karion, A, Kort, EA, Lamb, BK, Lauvaux, T, Maasakkers, JD, Marchese, AJ, Omara, M, Pacala, SW, Peischl, J, Robinson, AL, Shepson, PB, Sweeney, C, Townsend-Small, A, Wofsy, SC and **Hamburg, SP.** 2018. Assessment of methane emissions from the U.S. oil and gas supply chain. *Science* **361**: 186–188. DOI: https://doi.org/10.1126/science.aar7204

Balcombe, P, Brandon, NP and **Hawkes, AD.** 2018. Characterising the distribution of methane and carbon dioxide emissions from the natural gas supply chain. *J. Clean. Prod.* **172**: 2019–2032. DOI: https://doi.org/10.1016/j.jclepro.2017.11.223

Bares, R, Mitchell, L, Fasoli, B, Bowling, D, Catherine, D, Garcia, M, Eng, B, Ehleringer, J and **Lin, JC.**

2019. The Utah urban carbon network (UUCON) and Uintah Basin greenhousse gas networks: Instrumentation, data, and measurement uncertainty. *Earth Sys. Sci. Data Discuss.* DOI: https://doi.org/10.5194/essd-2018-148

Barkley, ZR, Lauvaux, T, Davis, KJ, Deng, A, Cao, Y, Sweeney, C, Martins, D, Miles, NL, Richardson, SJ, Murphy, T, Cervone, G, Karion, A, Schwietzke, S, Smith, M, Kort, EA and **Maasakkers, JD.** 2017. Quantifying methane emissions from natural gas production in northeastern Pennsylvania. *Atmos. Chem. Phys. Discuss.* 1–53. http://www.atmos-chem-phys-discuss.net/acp-2017-200/. DOI: https://doi.org/10.5194/acp-2017-200

Benjamin, SG, Weygandt, SS, Brown, JM, Hu, M, Alexander, CR, Smirnova, TG, Olson, JB, James, EP, Dowell, DC, Grell, GA, Lin, H, SE., Peckham, Smith, TL, Moninger, WR, Kenyon, JS and **Manikin, GS.** 2016. A North American hourly assimilation and model forecast cycle: the rapid refresh. *Mon. Weather Rev.* **144**: 1669–1694. http://journals.ametsoc.org/doi/10.1175/MWR-D-15-0242.1. DOI: https://doi.org/10.1175/MWR-D-15-0242.1

Bruhwiler, LM, Basu, S, Bergamaschi, P, Bousquet, P, Dlugokencky, E, Houweling, S, Ishizawa, M, Kim, H, Locatelli, R, Maksyutov, S, Montzka, S, Pandey, S, Patra, PK, Petron, G, Saunois, M, Sweeney, C, Schwietzke, S, Tans, P and **Weatherhead, EC.** 2017. U.S. CH_4 emissions from oil and gas production: have recent large increases been detected?. *J. Geophys. Res. Atmos.* **122**: 4070–4083. DOI: https://doi.org/10.1002/2016JD026157

Burnham, A, Han, J, Clark, CE, Wang, M, Dunn, JB and **Palou-Rivera, I.** 2012. Life-cycle greenhouse gas emissions of shale gas, natural gas, coal, and petroleum. *Environ. Sci. Technol.* **46**: 619–627. DOI: https://doi.org/10.1021/es201942m

Caulton, DR, Shepson, PB, Santoro, RL, Sparks, JP, Howarth, RW, Ingraffea, AR, Cambaliza, MOL, Sweeney, C, Karion, A, Davis, KJ, Stirm, BH, Montzka, SA and **Miller, BR.** 2014. Toward a better understanding and quantification of methane emissions from shale gas development. *Proc. Natl. Acad. Sci. U. S. A.* **111**: 6237–6242. DOI: https://doi.org/10.1073/pnas.1316546111

Connell, EO, Risk, D, Atherton, E, Bourlon, E, Baillie, J, Lowry, D and **Johnson, J.** 2019. Methane emissions from contrasting production regions within Alberta, Canada: implications under incoming federal methane regulations. *Elem. Sci. Anthr.* **7**: 1–13. DOI: https://doi.org/10.1525/elementa.341

Duncan, BN, Prados, AI, Lamsal, LN, Liu, Y, Streets, DG, Gupta, P, Hilsenrath, E, Kahn, RA, Nielsen, JE, Beyersdorf, AJ, Burton, SP, Fiore, AM, Fishman, J, Henze, DK, Hostetler, CA, Krotkov, NA, Lee, P, Lin, M, Pawson, S, Pfister, G, Pickering, KE, Pierce, RB, Yoshida, Y and **Ziemba, LD.** 2014. Satellite data of atmospheric pollution for U.S. air quality applications: examples of applications, summary of data end-user resources, answers to FAQs, and common mistakes to avoid. *Atmos. Environ.* **94**: 647–662. DOI: https://doi.org/10.1016/j.atmosenv.2014.05.061

Edwards, PM, Brown, SS, Roberts, JM, Ahmadov, R, Banta, RM, De Gouw, JA, Dube, WP, Field, RA, Flynn, JH, Gilman, JB, Graus, M, Helmig, D, Koss, A, Langford, AO, Lefer, BL, Lerner, BM, Li, R, Li, SA, McKeen, A, Murphy, SM, Parrish, DD, Senff, CJ, Soltis, J, Stutz, J, Sweeney, C, Thompson, CR, Trainer, MK, Tsai, C, Veres, PR, Washenfelder, RA, Warneke, C, Wild, RJ, Young, CJ, Yuan, B and **Zamora, R.** 2014. High winter ozone pollution from carbonyl photolysis in an oil and gas basin. *Nature* **514**: 351–354. DOI: https://doi.org/10.1038/nature13767

Fann, N, Baker, KR, Chan, EAW, Eyth, A, Macpherson, A, Miller, E and **Snyder, J.** 2018. Assessing human health $PM_{2.5}$ and ozone impacts from U.S. oil and natural gas sector emissions in 2025. *Environ. Sci. Technol.* **52**. DOI: https://doi.org/10.1021/acs.est.8b02050

Foster, CS, Crosman, ET, Holland, L, Mallia, DV, Fasoli, B, Bares, R, Horel, J and **Lin, JC.** 2017. Confirmation of elevated methane emissions in Utah's Uintah Basin with ground-based observations and a high-resolution transport model. *J. Geophys. Res. Atmos.* **122**: 26–44. DOI: https://doi.org/10.1002/2017JD027480

Goetz, JD, Avery, A, Werden, B, Floerchinger, C, Fortner, EC, Wormhoudt, J, Massoli, P, Herndon, SC, Kolb, CE, Knighton, WB, Peischl, J, Warneke, C, de Gouw, JA, Shaw, SL and **Decarlo, PF.** 2017. Analysis of local-scale background concentrations of methane and other gas-phase species in the Marcellus Shale. *Elem. Sci. Anthr.* **5**: 1–20. DOI: https://doi.org/10.1017/CBO9781107415324.004

Helmig, D, Thompson, CR, Evans, J, Boylan, P, Hueber, J and **Park, JH.** 2014. Highly elevated atmospheric levels of volatile organic compounds in the uintah basin, Utah. *Environ. Sci. Technol.* **48**: 4707–4715. DOI: https://doi.org/10.1021/es405046r

Horel, JD, Splitt, M, Dunn, L, Pechmann, B, White, C, Lazarus, S, Slemmer, J, Zaff, D and **Burks, J.** 2002. Mesowest: cooperative mesonets in the western United States. *Bull. Am. Meteorol. Soc.* **40**. DOI: https://doi.org/10.1175/1520-0477(2002)083<0211:MCMITW>2.3.CO;2

Howarth, RW. 2014. A bridge to nowhere: methane emissions and the greenhouse gas footprint of natural gas. *Energy Sci. Eng.* **2**: 47–60. DOI: https://doi.org/10.1002/ese3.35

Kang, M, Kanno, CM, Reid, MC, Zhang, X, Mauzerall, DL, Celia, MA, Chen, Y and **Onstott, TC.** 2014. Direct measurements of methane emissions from abandoned oil and gas wells in Pennsylvania. *Proc. Natl. Acad. Sci. U. S. A.* **111**: 18173–18177. DOI: https://doi.org/10.1073/pnas.1408315111

Karion, A, Sweeney, C, Kort, EA, Shepson, PB, Brewer, A, Cambaliza, M, Conley, SA, Davis, K, Deng, A, Hardesty, M, Herndon, SC, Lauvaux, T, Lavoie, T,

Lyon, D, Newberger, T, Petron, G, Rella, C, Smith, M, Wolter, S, Yacovitch, TI and **Tans, P.** 2015. Aircraft-based estimate of total methane emissions from the Barnett shale region. *Environ. Sci. Technol.* **49**: 8124–8131. DOI: https://doi.org/10.1021/acs.est.5b00217

Karion, A, Sweeney, C, Petron, G, Frost, G, Hardesty, RM, Kofler, J, Miller, BR, Newberger, T, Wolter, S, Banta, R, Brewer, A, Dlugokencky, E, Lang, P, Montzka, SA, Schnell, R, Tans, P, Trainer, M, Zamora, R and **Conley, S.** 2013. Methane emissions estimate from airborne measurements over a western United States natural gas field. *Geophys. Res. Lett.* **40**: 4393–4397. DOI: https://doi.org/10.1002/grl.50811

Koss, AR, De Gouw, J, Warneke, C, Gilman, JB, Lerner, BM, Graus, M, Yuan, B, Edwards, P, Brown, SS, Wild, R, Roberts, JM, Bates, TS and **Quinn, PK.** 2015. Photochemical aging of volatile organic compounds associated with oil and natural gas extraction in the Uintah Basin, UT, during a wintertime ozone formation event. *Atmos. Chem. Phys.* **15**: 5727–5741. DOI: https://doi.org/10.5194/acp-15-5727-2015

Kotthaus, S, O'Connor, E, Münkel, C, Charlton-Perez, C, Haeffelin, M, Gabey, AM and **Grimmond, CSB.** 2016. Recommendations for processing atmospheric attenuated backscatter profiles from Vaisala CL31 ceilometers. *Atmos. Meas. Tech.* **9**: 3769–3791. DOI: https://doi.org/10.5194/amt-9-3769-2016

Lareau, NP, Crosman, E, Whiteman, CD, Horel, JD, Hoch, SW, Brown, WOJ and **Horst, TW.** 2013. The persistent cold-air pool study. *Bull. Am. Meteorol. Soc.* **94**: 51–63. DOI: https://doi.org/10.1175/BAMS-D-11-00255.1

Lavoie, TN, Shepson, PB, Cambaliza, MOL, Stirm, BH, Conley, S, Mehrotra, S, Faloona, IC and **Lyon, D.** 2017. Spatiotemporal variability of methane emissions at oil and natural gas operations in the Eagle Ford Basin. *Environ. Sci. Technol.* **51**: 8001–8009. DOI: https://doi.org/10.1021/acs.est.7b00814

Lin, JC, Gerbig, C, Wofsy, SC, Andrews, AE, Daube, BC, Davis, KJ and **Grainger, CA.** 2003. A near-field tool for simulating the upstream influence of atmospheric observations: The Stochastic Time-Inverted Lagrangian Transport (STILT) model. *J. Geophys. Res.* **108**. DOI: https://doi.org/10.1029/2002JD003161

Lyman, S and **Shorthill, H.** 2013. Final report: Uinta Basin winter ozone and air quality study. http://rd.usu.edu/files/uploads/ubos_2010-11_final_report.pdf.

Lyman, S and **Tran, T.** 2015. Inversion structure and winter ozone distribution in the Uintah Basin, Utah, U.S.A. *Atmos. Environ.* **123**: 156–165. DOI: https://doi.org/10.1016/j.atmosenv.2015.10.067

Maasakkers, JD, Jacob, DJ, Sulprizio, MP, Turner, AJ, Weitz, M, Wirth, T, Hight, C, De Figueiredo, M, Desai, M, Schmeltz, R, Hockstad, L, Bloom, AA, Bowman, KW, Jeong, S and **Fischer, ML.** 2016. Gridded national inventory of U.S. methane emissions. *Environ. Sci. Technol.* **50**: 13123–13133. DOI: https://doi.org/10.1021/acs.est.6b02878

Mansfield, ML and **Hall, CF.** 2018. A survey of valleys and basins of the western United States for the capacity to produce winter ozone. *J. Air Waste Manage. Assoc.* **68**: 909–919. DOI: https://doi.org/10.1080/10962247.2018.1454356

Matichuk, R, Tonnesen, G, Luecken, D, Gilliam, R, Napelenok, SL, Baker, KR, Schwede, D, Murphy, B, Helmig, D, Lyman, SN and **Roselle, S.** 2017. Evaluation of the community multiscale air quality model for simulating winter ozone formation in the Uinta Basin. *J. Geophys. Res. Atmos.* **122**: 13,545–13,572. DOI: https://doi.org/10.1002/2017JD027057

Miller, SM, Wofsy, SC, Michalak, AM, Kort, EA, Andrews, AE, Biraud, SC, Dlugokencky, EJ, Eluszkiewicz, J, Fischer, ML, Janssens-Maenhout, G, Miller, BR, Miller, JB, Montzka, SA, Nehrkorn, T and **Sweeney, C.** 2013. Anthropogenic emissions of methane in the United States. *PNAS* **110**: 20018–20022. DOI: https://doi.org/10.1073/pnas.1314392110

Neemann, EM, Crosman, ET, Horel, JD and **Avey, L.** 2015. Simulations of a cold-air pool associated with elevated wintertime ozone in the Uintah Basin, Utah. *Atmos. Chem. Phys.* **15**: 135–151. DOI: https://doi.org/10.5194/acp-15-135-2015

Nehrkorn, T, Eluszkiewicz, J, Wofsy, SC, Lin, JC, Gerbig, C, Longo, M and **Freitas, S.** 2010. Coupled weather research and forecasting-stochastic time-inverted lagrangian transport (WRF-STILT) model. *Meteorol. Atmos. Phys.* **107**: 51–64. DOI: https://doi.org/10.1007/s00703-010-0068-x

Nisbet, EG, Dlugokencky, EJ, Manning, MR, Lowry, D, Fisher, RE, France, JL, Michel, SE, Miller, JB, White, JWC, Vaughn, B, Bousquet, P, Pyle, JA, Warwick, NJ, Cain, M, Brownlow, R, Zazzeri, G, Lanoisellé, M, Manning, AC, Gloor, E, Worthy, DEJ, Brunke, E-G, Labuschagne, C, Wolff, EW and **Ganesan, AL.** 2016. Rising atmospheric methane: 2007–2014 growth and isotopic shift. *Glob. Biogeochem. Cy.* **30**: 1356–1370. DOI: https://doi.org/10.1002/2016GB005406

Oltmans, SJ, Karion, A, Schnell, RC, Pétron, G, Helmig, D, Montzka, SA, Wolter, S, Neff, D, Miller, BR, Hueber, J, Conley, S, Johnson, BJ and **Sweeney, C.** 2016. O_3, CH_4, CO_2, CO, NO_2 and NMHC aircraft measurements in the Uinta Basin oil and gas region under low and high ozone conditions in winter 2012 and 2013. *Elem. Sci. Anthr.* **4**: 000132. DOI: https://doi.org/10.12952/journal.elementa.000132

Omara, M, Zimmerman, N, Sullivan, MR, Li, X, Ellis, A, Cesa, R, Subramanian, R, Presto, AA and **Robinson, AL.** 2018. Methane emissions from natural gas production sites in the United States: data synthesis and national estimate. *Environ. Sci. Technol.* **52**: 12915–12925. DOI: https://doi.org/10.1021/acs.est.8b03535

Orellana, A, Laurenzi, IJ, Maclean, HL and **Bergerson, JA.** 2018. Statistically enhanced model of in situ

oil sands extraction operations: an evaluation of variability in greenhouse gas emissions. *Environ. Sci. Technol.* **52**: 947–954. DOI: https://doi.org/10.1021/acs.est.7b04498

Peischl, J, Karion, A, Sweeney, C, Kort, EA, Smith, ML, Brandt, AR, Yeskoo, T, Aikin, KC, Conley, SA, Gvakharia, A, Trainer, M, Wolter, S and **Ryerson, TB.** 2016. Locating and quantifying greenhouse gas emissions at a geological CO 2 storage site using atmospheric modeling and measurements. *J. Geophys. Res. Atmos.* **121**: 6101–6111. DOI: https://doi.org/10.1002/2015JD024631

Peischl, J, Ryerson, TB, Aiken, KC, Gilman, JA, Holloway, JS, Lerner, BM, Nadkarni, R, Neuman, JA, Nowak, JB, Trainer, M, Warneke, C and **Parrish, DD.** 2015. Quantifying atmospheric methane emissions from the Haynesville, Fayetteville, and northeastern Marcellus shale gas production regions. *J. Geophys. Res.* **120**: 2119–2139. DOI: https://doi.org/10.1002/2014JD022697

Petron, G, Frost, G, Miller, BR, Hirsch, AI, Montzka, SA, Karion, A, Trainer, M, Sweeney, C, Andrews, AE, Miller, L, Kofler, J, Bar-Ilan, A, Dlugokencky, EJ, Patrick, L, Moore, CT, Ryerson, TB, Siso, C, Kolodzey, W, Lang, PM, Conway, T, Novelli, P, Masarie, K, Hall, B, Guenther, D, Kitzis, D, Miller, J, Welsh, D, Wolfe, D, Neff, W and **Tans, P.** 2012. Hydrocarbon emissions characterization in the Colorado Front Range: a pilot study. *J. Geophys. Res. Atmos.* **117**: 1–19. DOI: https://doi.org/10.1029/2011JD016360

Robertson, AM, Edie, R, Snare, D, Soltis, J, Field, RA, Burkhart, MD, Bell, CS, Zimmerle, D and **Murphy, SM.** 2017. Variation in methane emission rates from well pads in four oil and gas basins with contrasting production volumes and compositions. *Environ. Sci. Technol.* **51**: 8832–8840. DOI: https://doi.org/10.1021/acs.est.7b00571

Sahoo, PK, Soltani, S, Wong, AKC and **Chen, YC.** 1988. A survey of thresholding techniques. *Comput. Vision, Graph. Process.* **41**: 233–260. DOI: https://doi.org/10.1016/0734-189X(88)90022-9

Saunois, M, Bousquet, P, Poulter, B, Peregon, A, Ciais, P, Canadell, JG, Dlugokencky, EJ, Etiope, G, Bastviken, D, Houweling, S, Janssens-Maenhout, G, Tubiello, FN, Castaldi, S, Jackson, RB, Alexe, M, Arora, VK, Beerling, DJ, Bergamaschi, P, Blake, DR, Brailsford, G, Brovkin, V, Bruhwiler, L, Crevoisier, C, Crill, P, Covey, K, Curry, C, Frankenberg, C, Gedney, N, Höglund-Isaksson, L, Ishizawa, M, Ito, A, Joos, F, Kim, H, Kleinen, T, Krummel, P, Lamarque, J, Langenfelds, R, Locatelli, R, Machida, T, Maksyutov, S, McDonald, KC, Marshall, J, Melton, JR, Morino, I, Naik, V, O'Doherty, S, Parmentier, FW, Patra, PK, Peng, C, Peng, S, Peters, GP, Piso, I, Prigent, C, Prinn, R, Ramonet, M, Riley, WJ, Saito, M, Santini, M, Schroeder, R, Simpson, IJ, Spahni, R, Steele, P, Takizawa, A, Thornton, BF, Tian, H, Tohjima, Y, Viovy, N, Voulgarakis, A, van Weele, M, van der Werf, GR, Weiss, R, Wiedinmyer, C, Wilton, DJ, Wiltshire, A, Worthy, D, Wunch, D, Xu, X, Yoshida, Y, Zhang, B, Zhang, Z and **Zhu, Q.** 2016. The global methane budget 2000–2012. *Earth Syst. Sci. Data* **8**: 679–751. DOI: https://doi.org/10.5194/essd-8-697-2016

Saunois, M, Bousquet, P, Poulter, B, Peregon, A, Ciais, P, Canadell, JG, Dlugokencky, EJ, Etiope, G, Bastviken, D, Houweling, S, Janssens-Maenhout, G, Tubiello, FN, Castaldi, S, Jackson, RB, Alexe, M, Arora, VK, Beerling, DJ, Bergamaschi, P, Blake, DR, Brailsford, G, Bruhwiler, L, Crevoisier, C, Crill, P, Covey, K, Frankenberg, C, Gedney, N, Höglund-Isaksson, L, Ishizawa, M, Ito, A, Joos, F, Ki, H, Kleinen, T, Krummel, P, Lamarque, J, Langenfelds, R, Locatelli, R, Machida, T, Maksyutov, S, Melton, JR, Morino, I, Naik, V, O'Doherty, S, Parmentier, FW, Patra, PK, Peng, C, Peng, S, Peters, GP, Pison, I, Prinn, R, Ramonet, M, Riley, WJ, Saito, M, Santini, M, Schroeder, R, Simpson, IJ, Spahni, R, Takizawa, A, Thornton, BF, Tian, H, Tohjima, Y, Viovy, N, Voulgarakis, A, Weiss, R, Wilton, DJ, Wiltshire, A, Worthy, D, Wunch, D, Xu, X, Yoshida, Y, Zhang, B, Zhang, Z and **Zhu, Q.** 2017. Variability and quasi-decadal changes in the methane budget over the period 2000–2012. *Atmos. Chem. Phys.* **17**: 11135–11161. DOI: https://doi.org/10.5194/acp-17-11135-2017

Schnell, RC, Johnson, BJ, Oltmans, SJ, Cullis, P, Sterling, C, Hall, E, Jordan, A, Helmig, D, Petron, G, Ahmadov, R, Wendell, J, Albee, R, Boylan, P, Thompson, CR, Evans, J, Hueb, J and **Park, J.** 2016. Quantifying wintertime boundary layer ozone production from frequent profile measurements in the Uinta Basin, UT, oil and gas region. *J. Geophys. Res. Atmos.* **121**: 11038–11054. DOI: https://doi.org/10.1002/2016JD024957

Schnell, RC, Oltmans, SJ, Neely, RR, Endres, MS, Molenar, JV and **White, AB.** 2009. Rapid photochemical production of ozone at high concentrations in a rural site during winter. *Nat. Geosci.* **2**: 120–122. DOI: https://doi.org/10.1038/ngeo415

Schwietzke, S, Petron, G, Conley, S, Pickering, C, Mielke-Maday, I, Dlugokencky, EJ, Tans, PP, Vaughn, T, Bell, C, Zimmerle, D, Wolter, S, King, CW, White, AB, Coleman, T, Bianco, L and **Schnell, RC.** 2017. Improved mechanistic understanding of natural gas methane emissions from spatially-resolved aircraft measurements. *Environ. Sci. Technol.* **51**: 7286–7294. DOI: https://doi.org/10.1021/acs.est.7b01810

Sheng, J, Jacob, DJ, Turner, AJ, Maasakkers, JD, Benmergui1, J, Bloom, AA, Arndt, C, Gautam, R, Zavala-Araiza, D, Boesch, H and **Parker, RJ.** 2018. 2010–2016 methane trends over Canada, the United States, and Mexico. *Atmos. Chem. Phys.* **18**: 12257–12267. DOI: https://doi.org/10.5194/acp-18-12257-2018

Subramanian, R, Williams, LL, Vaughn, TL, Zimmerle, D, Roscioli, JR, Herndon, SC, Yacovitch, TI,

Floerchinger, C, Tkacik, DS, Mitchell, AL, Sullivan, MR, Dallmann, TR and **Robinson, AL.** 2015. Methane emissions from natural gas compressor stations in the transmission and storage sector: Measurements and comparisons with the EPA greenhouse gas reporting program protocol. *Environ. Sci. Technol.* **49**: 3252–3261. DOI: https://doi.org/10.1021/es5060258

Taylor, JR. 1982. An introduction to error analysis: The study of uncertainties in physical measurements. Mill Valley, Calif: University Science Books.

Thompson, RL, Nisbet, EG, Pisso, I, Stohl, A, Blake, D, Dlugokencky, EJ, Helmig, D, White, JWC. 2018. Variability in atmospheric methane from fossil fuel and microbial sources over the last three decades. *Geophys. Res. Lett.* **45**: 11499–11508. DOI: https://doi.org/10.1029/2018GL078127

Tran, T, Tran, H, Mansfield, M, Lyman, S and **Crosman, E.** 2018. Four dimensional data assimilation (FDDA) impacts on WRF performance in simulating inversion layer structure and distributions of CMAQ-simulated winter ozone concentrations in Uintah Basin. *Atmos. Environ.* **177**: 75–92. DOI: https://doi.org/10.1016/j.atmosenv.2018.01.012

Turner, AJ, Frankenberg, C and **Kort, EA.** 2019. Interpreting contemporary trends in atmospheric methane. *Proc. Natl. Acad. Sci.* **116**: 2805–2813. DOI: https://doi.org/10.1073/pnas.1814297116

Turner, AJ, Frankenberg, C, Wennberg, PO and **Jacob, DJ.** 2017. Ambiguity in the causes for decadal trends in atmospheric methane and hydroxyl. *Proc. Natl. Acad. Sci.* **114**: 5367–5372. DOI: https://doi.org/10.1073/pnas.1616020114

Turner, AJ, Jacob, DJ, Benmergui, J, Wofsy, SC, Maasakkers, JD, Butz, A, Hasekamp, O and **Biraud, SC.** 2016. A large increase in U.S. methane emissions over the past decade inferred from satellite data and surface observations. *Geophys. Res. Lett.* **43**: 2218–2224. DOI: https://doi.org/10.1002/2016GL067987

Vaughn, TL, Bell, CS, Pickering, CK, Schwietzke, S, Heath, GA, Petron, G, Zimmerle, DJ, Schnell, RC and **Nummedal, D.** 2018. Temporal variability largely explains top-down/bottom-up difference in methane emission estimates from a natural gas production region. *Proc. Natl. Acad. Sci.* **115**: 11712–11717. DOI: https://doi.org/10.1073/pnas.1805687115

Whiteman, CD, Hoch, SW, Horel, JD and **Charland, A.** 2014. Relationship between particulate air pollution and meteorological variables in Utah's Salt Lake Valley. *Atmos. Environ.* **94**: 742–753. DOI: https://doi.org/10.1016/j.atmosenv.2014.06.012

Young, JS and **Whiteman, CD.** 2015. Laser ceilometer investigation of persistent wintertime cold-air pools in Utah's Salt Lake Valley. *J. Appl. Meteorol. Climatol.* **54**: 752–765. DOI: https://doi.org/10.1175/JAMC-D-14-0115.1

Yuan, B, Liggio, J, Wentzell, J, Li, SM, Stark, H, Roberts, JM, Gilman, J, Lerner, B, Warneke, C, Li, R, Leithead, A, Osthoff, HD, Wild, R, Brown, SS and **DeGouw, JA.** 2016. Secondary formation of nitrated phenols: Insights from observations during the Uintah Basin Winter Ozone Study (UBWOS) 2014. *Atmos. Chem. Phys.* **16**: 2139–2153. DOI: https://doi.org/10.5194/acp-16-2139-2016

How to cite this article: Foster, CS, Crosman, ET, Horel, JD, Lyman, S, Fasoli, B, Bares, R and Lin, JC. 2019. Quantifying methane emissions in the Uintah Basin during wintertime stagnation episodes. *Elem Sci Anth,* 7: 24. DOI: https://doi.org/10.1525/elementa.362

Domain Editor-in-Chief: Detlev Helmig, Institute of Alpine and Arctic Research, University of Colorado Boulder, US

Associate Editor: Brian Lamb, Washington State University, US

Knowledge Domain: Atmospheric Science

Part of an *Elementa* Special Feature: Oil and Natural Gas Development: Air Quality, Climate Science, and Policy

Submitted: 17 January 2019 **Accepted:** 09 May 2019 **Published:** 12 June 2019

ELEMENTA Science of the Anthropocene

Elem Sci Anth is a peer-reviewed open access journal published by University of California Press.

OPEN ACCESS